Forecasting the Exoplanet Yield and Observational Capabilities of the LIFE Mission: Literature Summary

Sona Davis, Department of Astronomy, Univeristy of Belgrade, Serbia

Contents

Introduction to the LIFE Mission

The Large Interferometer For Exoplanets (LIFE) is a proposed space-based mid-infrared nulling interferometer designed to detect and characterize terrestrial exoplanets in the habitable zones of nearby stars. Its primary scientific objectives include discovering Earth-like planets, characterizing their atmospheres, and searching for potential biosignature gases such as O_2, O_3, and PH_3.

Early studies estimated the exoplanet detection yield based on Kepler statistics (Kammerer & Quanz 2018), while subsequent work refined simulations and retrieval frameworks to provide more accurate predictions for various mission architectures and noise assumptions (Quanz et al. 2021; Glauser et al. 2024). Specific investigations of biosignature detectability and combined observational strategies with reflected-light missions have been explored (Angerhausen et al. 2023; Alei et al. 2024), as well as Bayesian approaches to interpret null results and optimize mission design (Angerhausen et al. 2025; Kammerer et al. 2022).

The following sections provide detailed summaries of seven key publications, highlighting their main assumptions, target selections, predicted yields, and scientific conclusions.

1 Kammerer & Quanz (2018) — "Simulating the exoplanet yield of a space-based mid-infrared interferometer based on Kepler statistics"

Reference

J. Kammerer & S. P. Quanz (2018). A&A 609, A4. (arXiv:1707.06820)

Summary

This work uses Monte Carlo simulations (2000 simulated planetary systems) based on Kepler-derived occurrence rates to estimate the detection yield of a space-based mid-infrared (MIR) nulling interferometer. The study explores the detectability of planets with radii between 0.5 and $6\,R_\oplus$ across three MIR bands (5.6, 10.0 and $15.0\,\mu m$) and computes expected yields for a sample of nearby stars ($d < 20\,pc$).

Key assumptions

- Planet occurrence as extrapolated from Kepler (period/radius distributions).

- Thermal equilibrium and blackbody emission for planets.

- Uniformly distributed geometric albedos for reflected-light considerations (where needed).

- Instrument performance assumptions: spatial resolution and sensitivity tuned to three MIR bands; throughputs assumed several times worse than JWST in a conservative case.

- Stellar sample: ~ 326 nearby stars within $20\,pc$.

Methods

Monte Carlo population synthesis + instrument simulator evaluating detectability per band and per simulated system; identification of best target stars and sensitivity tests versus instrumental/astrophysical parameters.

Exoplanet yield (reported)

- Median/nominal yield $\sim 315^{+113}_{-77}$ planets (0.5–$6\,R_\oplus$) detectable in at least one band in ~ 0.52 years of mission time under the cited throughput/overhead assumptions.

- ~ 85 planets would meet the paper's "habitable" criterion (0.5–$1.75\,R_\oplus$ and $T_{eq} \in [200, 450]\,K$).

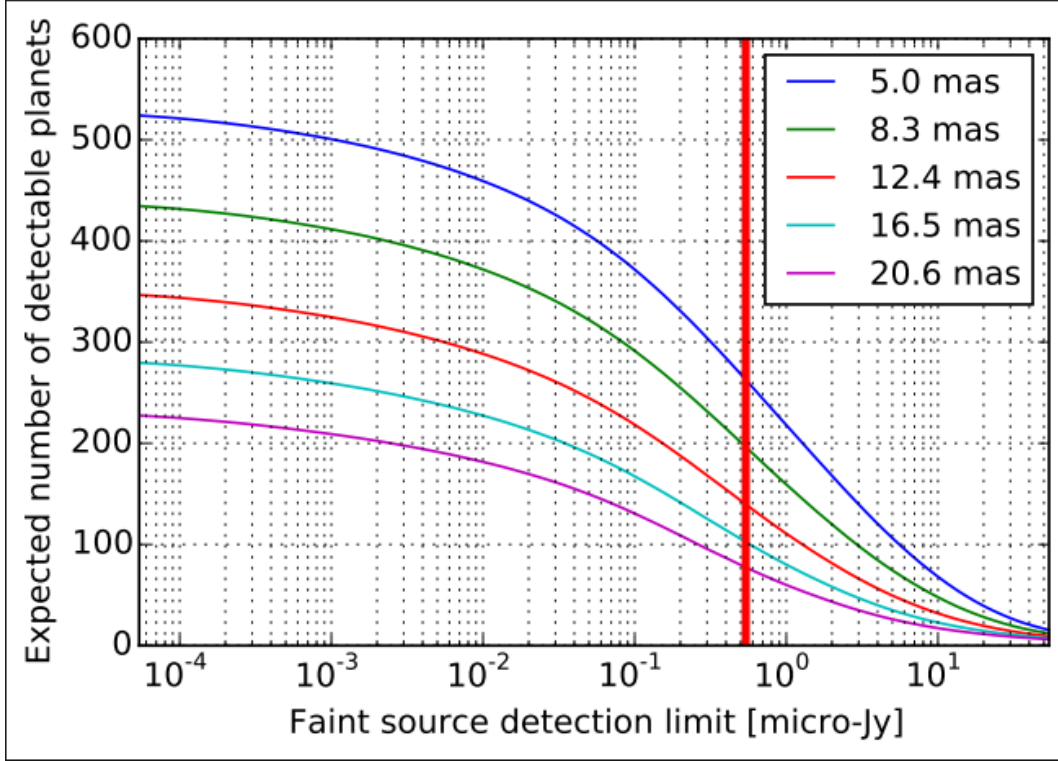- Discovery phase realistically requires ~ 2–3 years when accounting for stellar leakage and exozodiacal dust effects.

Figure 1: expected number of detectable exoplanets (with radii ¡ 6 REarth) as a function of the faint source detection limit Flim for the 10 μm filter. The five curves represent various nulling baselines, i.e., various IWAs ranging from 5.0 mas (baseline value) to 20.6 mas. The red vertical line indicates our baseline detection limit of Flim, F1000W = 0.54μJy..

Figure 2: Left: expected number of detectable exoplanets (with radii ¡6 REarth) for each individual host star from our star catalog. Each of the 326 host stars is represented by one bin of the histogram (see color code for the different spectral types in the figure legend). This plot contains all exoplanets that can be detected in at least one of the three filters used in this work (5.6 μ m, 10 μm, 15 μm). Right: expected number of detectable exoplanets for each individual host star from our star catalog (left axis, as in the left panel), but sorted by completeness (right axis) overplotted as the transparent gray curve on the histogram.

Targets

Nearby stars within 20 pc (sample ~ 326 stars), prioritized by detectability metrics derived from simulations.

Exoplanet Yield and Parameters

Metric	Value / Notes
Total detectable planets (0.5–6 R$_\oplus$)	315^{+113}_{-77}
Rocky HZ planets (0.5–1.75 R$_\oplus$)	~ 85
Target stars	326 stars, < 20 pc, F/G/K/M
Wavelength bands	5.6, 10, 15 μm
Instrument throughput	Conservative estimates (several times worse than JWST)
Search phase duration	~ 0.52 yr

Table 1: Exoplanet yield and target summary for Kammerer & Quanz (2018).

Conclusions & implications

A MIR nulling interferometer can detect hundreds of planets (including many small planets) around nearby stars if instrumental sensitivity and throughput assumptions are met; the mission would identify promising candidates for follow-up spectroscopic characterization.

Limitations & uncertainties

Yields depend strongly on the assumed occurrence rates (extrapolation uncertainties), instrument throughput and time overheads, and assumptions about exozodiacal dust and stellar leakage. In addition, the simulations assume blackbody planetary emission and neglect atmospheric composition effects, which could impact the detectability of certain planets. The study also does not account for variability in stellar activity, which could affect the achievable null depth and signal-to-noise ratio, potentially reducing the effective detection yield.
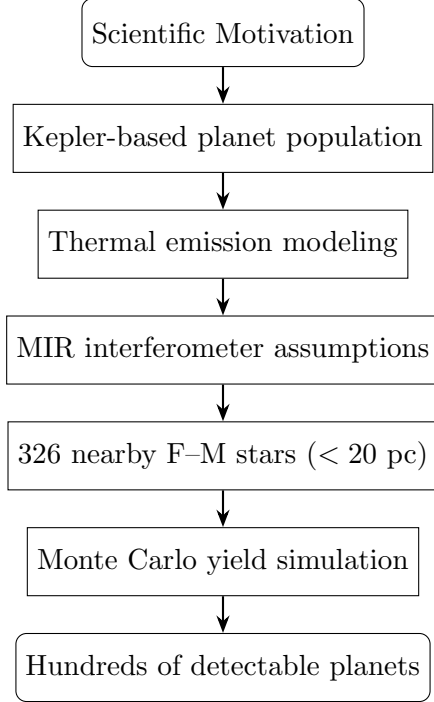
Figure 3: Flowchart summarizing Kammerer & Quanz (2018).

2 Quanz et al. (2021) — "LIFE I: Improved exoplanet detection yield estimates for a large mid-infrared space-interferometer mission"

Reference

S. P. Quanz et al. (2021), LIFE collaboration — arXiv:2101.07500 (A&A 664, A21 in later journal version).

Summary

This is the first comprehensive LIFE collaboration yield paper presenting an instrument simulator (LIFEsim) coupled with Monte Carlo synthetic planet populations (stars within 20 pc) to quantify the number and types of exoplanets detectable by a mid-IR nulling interferometer. The paper examines different aperture sizes, wavelength ranges and two observing-time distribution strategies.

Key assumptions

- Synthetic exoplanet populations based on Kepler occurrence statistics for planets between 0.5–$6\,R_\oplus$.

- Instrument concepts: array of four collectors ($2\,\text{m}$, $3.5\,\text{m}$ or $1\,\text{m}$ aperture options), a nuller/combiner, total instrument throughput baseline 5%, wavelength coverage 4–$18.5\,\mu$m for the primary case.

- Two observing time allocation strategies (broad vs. deep targeting).
- Full accounting for major astrophysical noise sources in LIFEsim.

Methods

Monte Carlo forward simulations with LIFEsim including astrophysical noise sources; yield computed for a 2.5-year search phase and different instrument configurations.
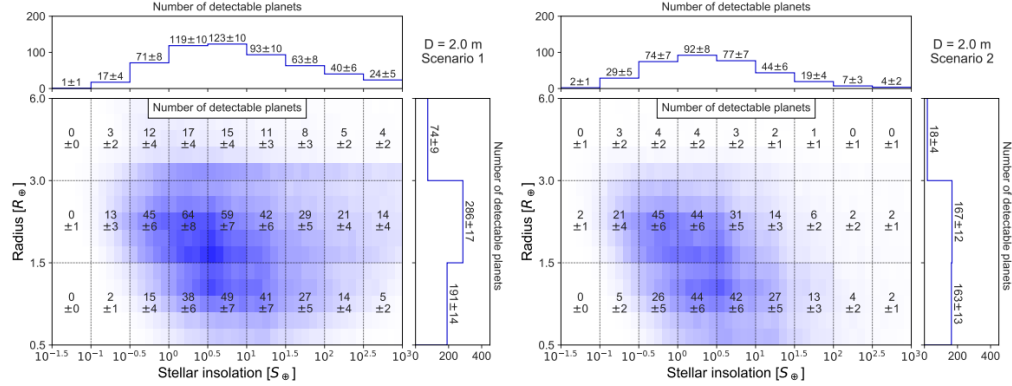

Figure 4: . Total exoplanet detection yield from our reference case scenario simulations (D = 2 m; $\lambda = 4$ 18.5 μm) in the radius vs. stellar insolation plane. The plots show the number of expected planet detections per grid cell, including the statistical 1- uncertainty from the Monte Carlo approach but excluding uncertainties in the exoplanet occurrence rates. Left panel: Scenario 1 (search phase optimized for maximizing the total number of exoplanets). Right panel: Scenario 2 (search phase optimized for maximizing the number of rocky eHZ exoplanets.)

Targets

Nearby main-sequence stars within 20 pc; yield results broken down by spectral type and prioritized target lists per observing strategy.

Exoplanet Yield

Aperture	Total planets	Rocky planets ($<$1.5 $R_\oplus$)	HZ rocky planets
1 m	315	~ 20	1–3
2 m	550	160	25–45
3.5 m	770	250	60–80

Table 2: Dependence of yields on aperture for Quanz et al. (2021). Stellar sample: 326 stars $<$ 20 pc, F/G/K/M types.

Conclusions & implications

A large MIR nulling interferometer (LIFE-like) can detect very large samples of small planets and tens of potentially rocky habitable-zone planets depending on aperture and throughput;

the concept is competitive with large single-aperture reflected-light missions in terms of detection yield for small planets.

Limitations & uncertainties

Strong dependence on aperture size and throughput; yields sensitive to assumed planet populations and observing strategy. The paper emphasizes instrument parameters that most influence yield (mirror diameter, throughput).
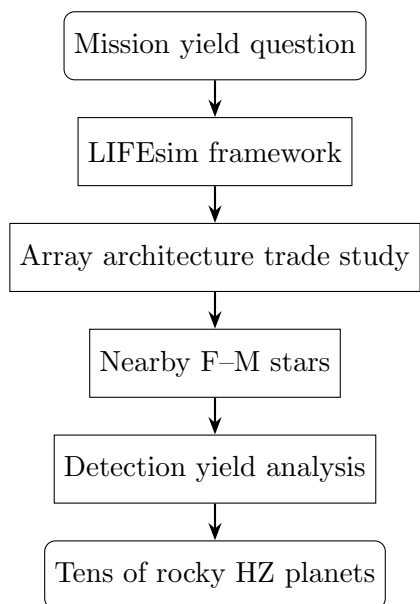
Mission yield question

↓

LIFEsim framework

↓

Array architecture trade study

↓

Nearby F–M stars

↓

Detection yield analysis

↓

Tens of rocky HZ planets

Figure 5: Flowchart summarizing Quanz et al. (2021).

3 Glauser et al. (2024) — "The Large Interferometer for Exoplanets (LIFE): a space mission for mid-infrared nulling interferometry" (SPIE proceedings)

Reference

A. M. Glauser et al. (2024), SPIE 13095; conference paper / mission overview (DTU-hosted PDF).

Summary

A mission-level description of LIFE: science goals, mission design drivers, formation-flying architecture, thermal and formation constraints, instrument concept and high-level performance trades. The paper focuses on mission feasibility, optical/formation constraints and system-level requirements.

Key assumptions

- Mission located at Sun–Earth L2 for formation-flying and thermal stability.

- Collector/combiners separation and formation control feasible with current/future formation-flying tech.

- Cryogenic instrument and thermal environment requirements consistent with MIR nulling operation.

Methods

Systems engineering, concept-of-operations, trades between collector size, combiner height, field-of-regard and modulation schemes; early design and feasibility analyses.

Targets

Mission is designed to observe nearby stars (within a few tens of parsecs) to detect and spectrally characterize thermal emission from small exoplanets.
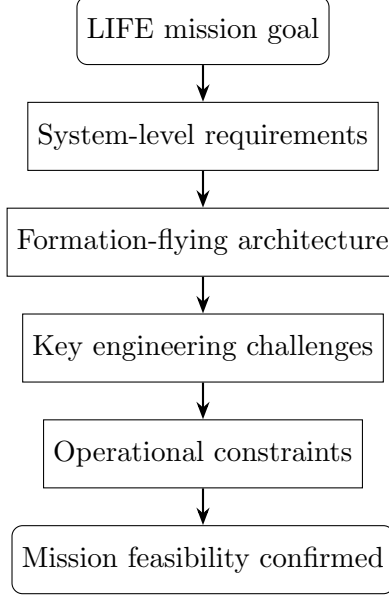
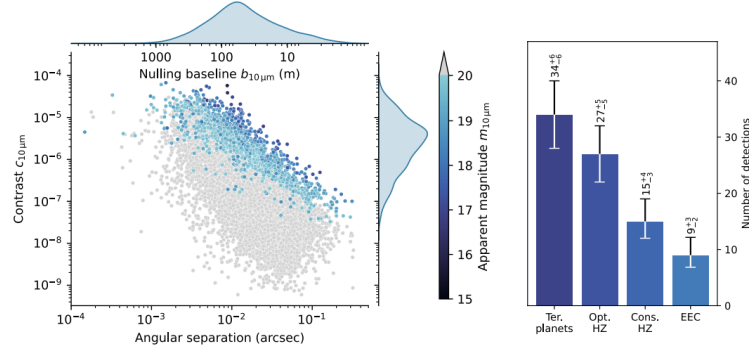Figure 6: Flowchart summarizing Glauser et al. (2024).

Figure 7: Left: Illustration of how the results of the Kepler mission inform key mission parameters of LIFE. Points plotted are an artificial rocky planet population based on Kepler statistics32, 37 occurring in their respective habitable zones generated using P-Pop.34 We plot their respective star-to-planet flux contrast ratio measured at 10 µm over the angular separation at which they occurred. The colors trace the planet's apparent 10 µm Vega-magnitude and planets with m10µm ¿ 20 are plotted in gray. The nulling baseline length required to achieve a certain angular resolution is shown. Right: Yield predictions with the setup specified in Table 1. The yields are based on artificial planet populations described in Kammerer et al. (2022).18 Shown are the expected number of detections around F-, G- and K-type stars within the distance up to 20 pc for all terrestrial exoplanets (0.5 $R_\oplus$ < Rp < 1.5 $R_\oplus$), terrestrial exoplanets in the optimistic and conservative habitable zone38 and for exo-Earth candidates (EEC, 0.8$R_\oplus$ < Rp < 1.4 $R_\oplus$ in conservative HZ)

Item	Value	Rationale or Comment
# collector spacecraft	4	Minimum number required for robustness against instrumental noise with baseline beam combiner.
Nulling baseline	10–100 m	Lower limit for nulling of nearest Sun-like stars; upper limit for M-type stars at 10 pc; lower bound sets minimum spacecraft separation.
Imaging baseline	60–600 m	Shifts planet modulation to higher frequencies to mitigate low-frequency instability noise; upper limit sets maximum spacecraft separation.
Combiner spacecraft	Out of plane	Full-sky field of regard; reduced complexity in collector spacecraft.
Modulation	Rotation & Phase chopping	Rotation improves planet localization and fuel efficiency; phase chopping calibrates detector and incoherent light.
Temperature	≤ 45 K	Reduces thermal emission from the collector mirror.
Beam combiner	Double Bracewell	High TRL bulk optics; good instability-noise suppression.
Wavelength coverage	6–16 µm (goal 4.5–18 µm)	Includes H_2O feature above 17 µm and resolves H_2O and CH_4 features at 7.7 µm.
Resolving power	> 100	Needed for CH_4 detection in Earth-like atmospheres.
Sensitivity*	$S_{10\mu m} = 0.4\,\mu$Jy (4 days)	Allows detection and characterization of 30 rocky HZ planets around Sun-like stars.
Contrast*	Null depth 10^{-5}; stability 10^{-8} rms	Required for faint thermal exoplanet signal detection.
Instrument temperature	≤ 15 K	Reduces thermal background from internal structure and optics.
Mission lifetime	≥ 5 years	Needed to detect and characterize the target sample of 30 rocky planets.

Table 3: Key mission parameters and requirements for LIFE

Conclusions & implications

LIFE as a mission concept is technically plausible but places stringent requirements on formation flying, cryogenics, and the optical/thermal design; the paper outlines engineering areas requiring technology maturation and provides mission-level input to the LIFE science simulations.

Limitations & uncertainties

Technical readiness of several subsystems (precision formation flying, cryogenic optics, nuller stability) and the consequent impact on achievable throughput and sensitivity; these system-level parameters feed back strongly into the yield estimates in the simulation papers.

4 Angerhausen et al. (2023) — "LIFE VIII: Where is the phosphine? Observing exoplanetary PH₃"

Reference

Summary

This paper evaluates detectability of PH_3 (phosphine) in exoplanet atmospheres using LIFEsim plus forward chemistry and radiative-transfer models. It explores a set of prototypical cases (warm giant, temperate super-Earths, Venus-like) and computes required integration times.

Key assumptions

- Representative atmospheric compositions (H_2-dominated, CO_2-dominated, Venus-like) and PH_3 abundances informed by literature/solar system analogues.

- Use of chemistry + radiative transfer forward models coupled to LIFEsim detection sensitivity.

- Distances and host-star types are representative (examples: G-star at $10\,\mathrm{pc}$, M-star hosts at $5\,\mathrm{pc}$).

Methods

Chemistry and radiative-transfer forward models were generated for illustrative scenarios, then passed to LIFEsim to compute SNR and integration times necessary for detection.

Results / Detection times

- Warm giant (G star, $10\,\mathrm{pc}$): PH_3 detection in $\sim 1\,\mathrm{hour}$ (LIFE).

- H_2 or CO_2 dominated temperate super-Earths (M star, $5\,\mathrm{pc}$): detection in $\sim 10\,\mathrm{hours}$.

- Venus-like twin at $5\,\mathrm{pc}$: even with extreme PH_3 concentrations, detection seems unlikely within $\sim 100\,\mathrm{hours}$.

- PH_3 is generally easier to detect with LIFE than with JWST by about an order of magnitude in required observing time for comparable cases.

Targets

Representative nearby targets across stellar types; the study identifies a sizable number of accessible objects for the observational classes considered.
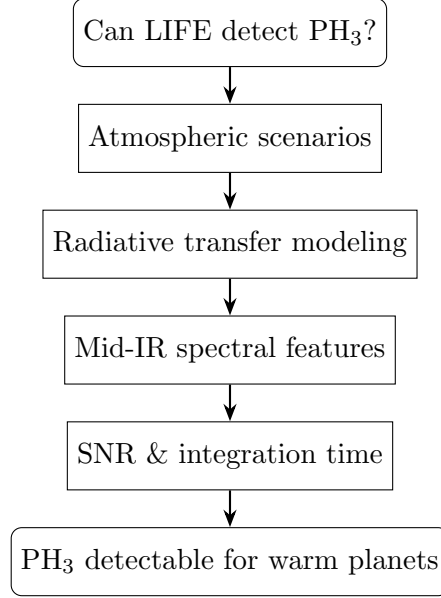
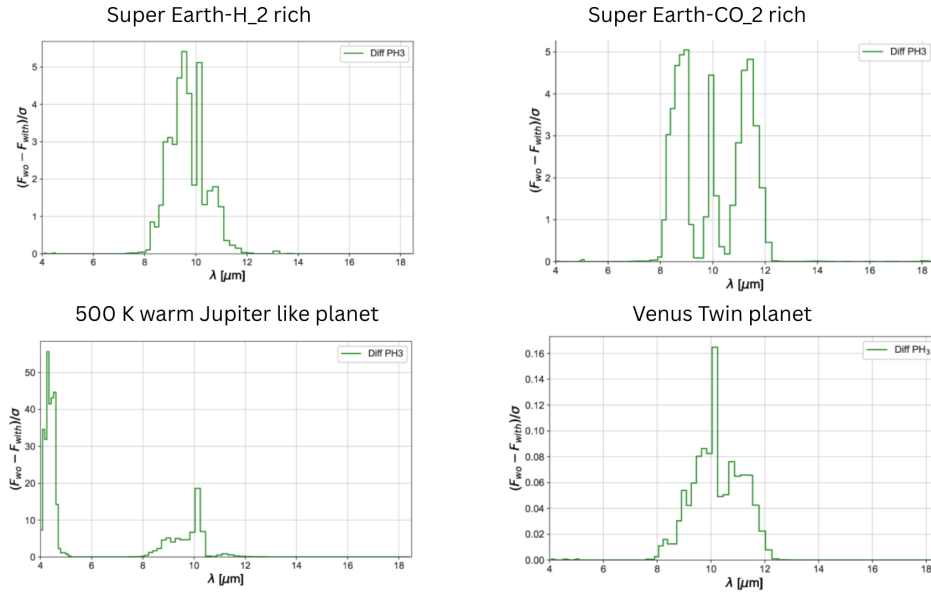Figure 8: Flowchart summarizing Angerhausen et al. (2023).

Figure 9: Statistical significance of the detected difference between atmospheric models with and without phosphine (PH_3) in simulated LIFE mid-infrared emission spectra for representative exoplanet scenarios. Top left: super-Earth ($10\,M_\oplus$, $1.75\,R_\oplus$) with a hydrogen-rich atmosphere orbiting an active M-dwarf after 10 hours of observation. Top right: super-Earth ($10\,M_\oplus$, $1.75\,R_\oplus$) with a carbon-dioxide-rich atmosphere orbiting an active M-dwarf after 10 hours of observation. Bottom left: warm Jupiter-like planet (500 K) after 1 hour of observation. Bottom right: Venus-twin planet after 100 hours of observation. The significance curves quantify the wavelength-dependent confidence with which PH_3 can be distinguished from PH_3-free atmospheric models for each planetary class.

13

Exoplanet Yield

Target Type	Distance / Host	PH$_3$ Detection Time (hr)
Warm giant	10 pc / G-star	~ 1
Temperate super-Earth	5 pc / M-star	~ 10
Venus analog	5 pc / G-star	~ 100 (unlikely)

Table 4: PH$_3$ detectability for representative targets in Angerhausen et al. (2023).

Conclusions & implications

PH$_3$ could be detected in favorable classes (warm giants, some temperate super-Earths) with short to moderate integration times using a LIFE-like mission; detection for Venus analogs is challenging. The paper provides prioritization guidance for PH$_3$ parameter space and inputs for further retrieval work.

Limitations & uncertainties

Model-dependent chemistry and uncertainties about realistic PH$_3$ production mechanisms; target abundance/distribution uncertain; forward-model and retrieval follow-up required.

5   Alei et al. (2024) — "LIFE XIII: The value of combining thermal emission and reflected light for the characterization of Earth twins"

Reference

Summary

This study compares atmospheric retrieval performance for a cloud-free Earth twin at 10 pc observed by an HWO-like reflected-light mission and a LIFE-like MIR thermal-emission mission, both separately and jointly. It quantifies the additional constraints on atmospheric composition, temperature profile and planetary parameters enabled by combining datasets.

Key assumptions

- Cloud-free Earth twin around a Sun-like star at 10 pc.

- Baseline spectral resolutions and assumed noise models aligned with current HWO and LIFE concept baselines.

- Two noise complexity levels considered (simpler and more realistic).

Methods

Bayesian atmospheric retrievals on simulated spectra from HWO-like (UV/VIS/NIR) and LIFE-like (MIR) concepts, performed individually and jointly.

Results

- HWO alone: constrains H_2O, O_2, O_3 but with large uncertainty in temperature profile ($\sim 100\,K$).

- LIFE alone: constrains CO_2, H_2O, O_3 and gives good constraints on thermal structure and surface temperature (uncertainty $\sim 10\,K$).

- Joint retrievals (HWO + LIFE): much tighter constraints on CO_2, H_2O, O_2, O_3, thermal profile and planetary parameters; some improvement on CH_4 and CO detection limits.
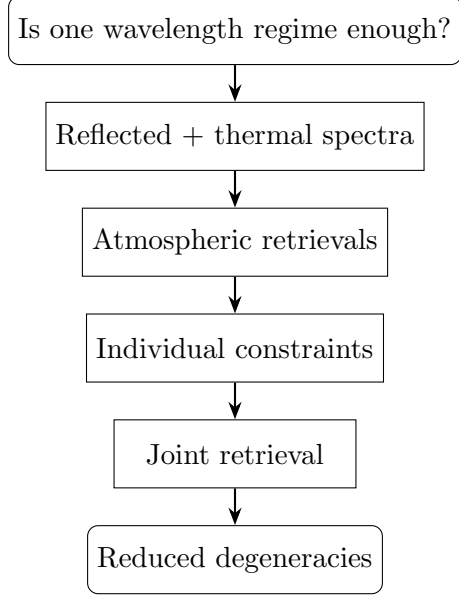
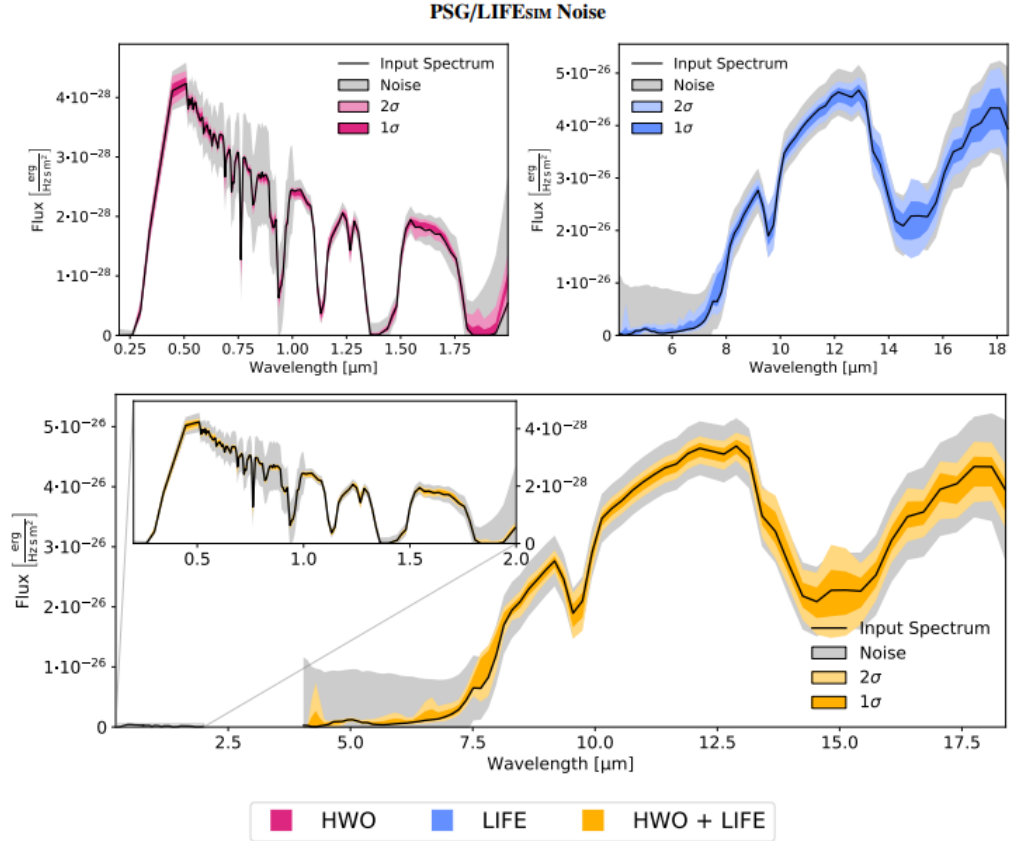Figure 10: Flowchart summarizing Alei et al. (2024).

Figure 11: Retrieved spectra for the third retrieval set (PSG/LIFEsim noise). Left panel: pure HWO retrieval (magenta); central panel: pure LIFE retrieval (blue); right panel: combined HWO+LIFE retrieval (yellow). In all panels, the 2-σ and 1-σ confidence intervals are shown with increasingly darker hues. The input spectra (black lines) and their associated uncertainties (gray-shaded error bars) are overplotted for comparison.

Targets

A notional Earth twin at 10 pc (cloud-free scenario) used as illustrative example; conclusions generalize to temperate terrestrial planets observed jointly by reflected-light and thermal-emission missions.

Retrieval Constraints

Observation Type	Constrained Species / Temp	Uncertainty
HWO only	H_2O, O_2, O_3	Temp $\sim$100 K
LIFE only	CO_2, H_2O, O_3	Temp $\sim$10 K
HWO + LIFE	H_2O, CO_2, O_2, O_3, thermal profile	Tight constraints, improved CH_4/CO limits

Table 5: Comparison of retrieval performance for Earth-twin analog in Alei et al. (2024).

Conclusions & implications

Thermal emission (LIFE) and reflected light (HWO) provide complementary and synergistic constraints — joint observations significantly improve characterization and biosignature interpretation compared to either approach alone.

Limitations & uncertainties

Study used a cloud-free Earth twin; clouds and aerosols can alter retrieval outcomes in practice. Noise and instrument systematic assumptions affect exact constraint levels.

6 Angerhausen et al. (2025) — "What if we find nothing? Bayesian analysis of the statistical information of null results..."

Reference

D. Angerhausen et al. (2025). AJ 169, 5 (arXiv:2504.06779).

Summary

This paper develops a Bayesian framework to evaluate what scientifically meaningful constraints can be drawn from null results (no detections of a binary observable) in future exoplanet habitability or biosignature surveys. The authors compute how many high-quality observations are needed to place strong upper limits on occurrence fractions (e.g., fraction of planets that are habitable/inhabited).

Key assumptions

- The observable is binary (detected / not detected) per planet.

- Both "perfect" and "imperfect" observation cases considered (perfect = 100% detection/exclusion confidence per target).

- Priors on the occurrence rate vary; posterior behavior is explored across priors.

Results

- $\sim$ 20–50 "perfect" observations suffice to draw conclusions that are largely independent of priors.

- To achieve a 99.9% upper limit $\eta_{\mathrm{obs}} \leq 0.2$ (0.1) requires roughly $N \approx 40$ (80) high-quality observations.

- For imperfect observations, biases and interpretation uncertainties reduce the constraining power; careful sample selection and high-confidence detection/exclusion per target is crucial.

- LIFE and HWO mission predicted yields are in the regime where meaningful upper limits / inferences become possible, provided observational quality and sample selection are adequate.
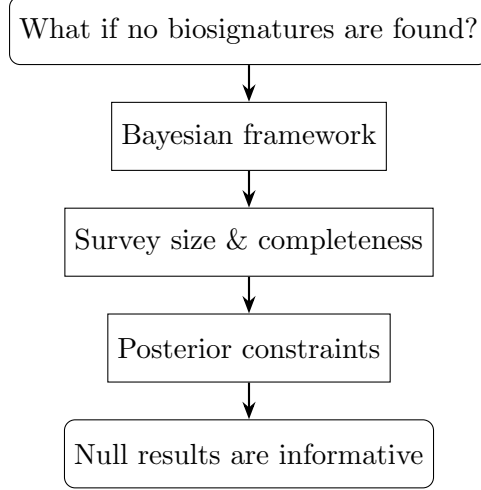
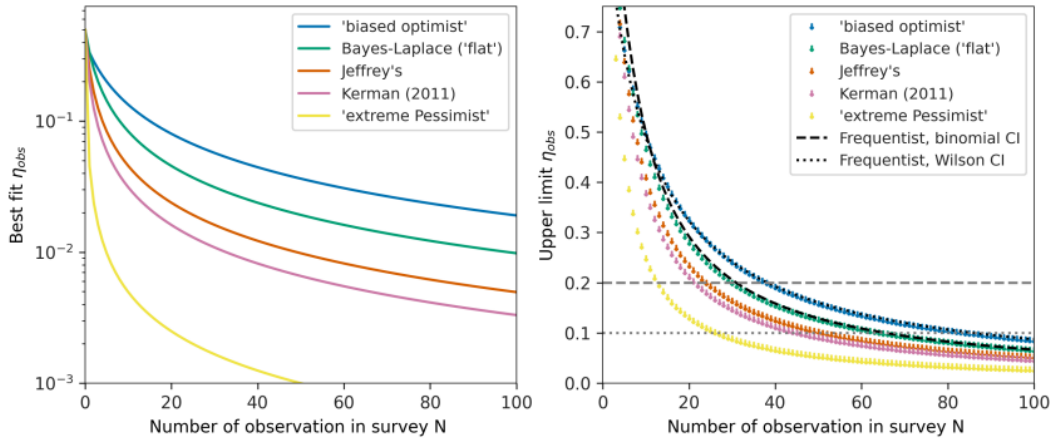Figure 12: Flowchart summarizing Angerhausen et al. (2025).

Figure 13: Final results for the case of a null-result survey of "perfect" observations. **Left:** Best fit from Bayesian analysis for the fraction η_{obs} as a function of the number N of non-detections. The Frequentist best fit corresponds to $\hat{\eta}_{\mathrm{MLE}} = 0$, and hence cannot be represented in this plot. **Right:** 99.9% upper limits derived from the credible intervals of the posteriors for the different prior beliefs. We also compare Bayesian to Frequentist uncertainty assessments by including both an exact binomial confidence interval and a Wilson confidence interval based on a normal approximation. In order to exclude scenarios with $\eta_{\mathrm{obs}} > 0.2$ and 0.1 with 99% confidence, more than ~ 40 or 80 individual "perfect" observations, respectively, would be required. As discussed in Section 2.2, the "optimistic" priors produce posteriors with higher values whereas the "pessimistic" priors are at the lower end of the spectrum.

Sample / Constraint Table

Scenario	Required Number of Observations
Perfect observations, $\eta_{\mathrm{obs}} \leq 0.2$	$N \approx 40$
Perfect observations, $\eta_{\mathrm{obs}} \leq 0.1$	$N \approx 80$
Imperfect observations	Increased sample; depends on detection confidence
Mission predicted yield (LIFE/HWO)	Allows meaningful upper limits if high-quality per-target SNR

Table 6: Sample size guidance for null-result surveys from Angerhausen et al. (2025).

Conclusions & implications

Null results are scientifically valuable: a sufficiently large, well-characterized survey can place tight constraints on the frequency of habitable/inhibited planets and biosignatures. The paper provides guidance on required sample sizes and the importance of per-target detection confidence.

Limitations & uncertainties

Real observations are never "perfect": instrument systematics, interpretation uncertainty, and target selection biases must be folded into real survey planning to ensure the theoretical sample-size requirements are met.

7 Kammerer et al. (2022) — "LIFE VI: Detecting rocky exoplanets in the habitable zones of Sun-like stars"

Reference

J. Kammerer et al. (2022). A&A 668, A52 (arXiv:2210.01782).

Summary

Focused on Sun-like and FGK star samples, this paper provides yield estimates for rocky planets in optimistic/optimistic HZs of Sun-like stars. It examines sensitivity to mirror diameter, throughput, exozodiacal dust level, and the accessible wavelength range.

Key assumptions

- Kepler-derived rocky planet occurrence rates extrapolated to the nearby-star sample.

- LIFEsim with astrophysical noise sources; instrumental noise sources not included in some simulations (conservative approach).

- Mirror diameter scalings tested ($1\,m$, $2\,m$, $3.5\,m$) and throughput variations.

Results

- For four $2\,m$ collectors, 5% throughput, and 2.5-year search phase: LIFE could detect between $\sim$ 10–16 rocky planets (0.5–$1.5\,R_\oplus$) within the optimistic HZ (average) or $\sim$ 5–34 including 1σ uncertainties.

- Exo-Earth candidates (EECs) estimates: $\sim$ 4–6 (average) within the optimistic HZ, or $\sim$ 1–13 including 1σ uncertainties.

- Yields increase with aperture roughly as $Y \propto D^{3/2}$ and strongly with total throughput; yields are weakly dependent on exozodiacal dust level and accessible wavelength range.

- With a larger FGK sample, yields rise to $\sim$ 16–22 rocky planets in optimistic HZ and $\sim$ 5–8 EECs (average).
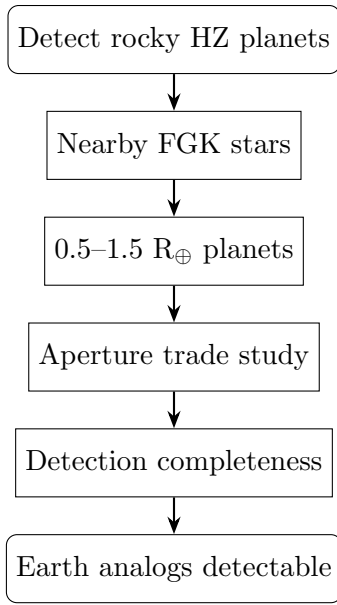
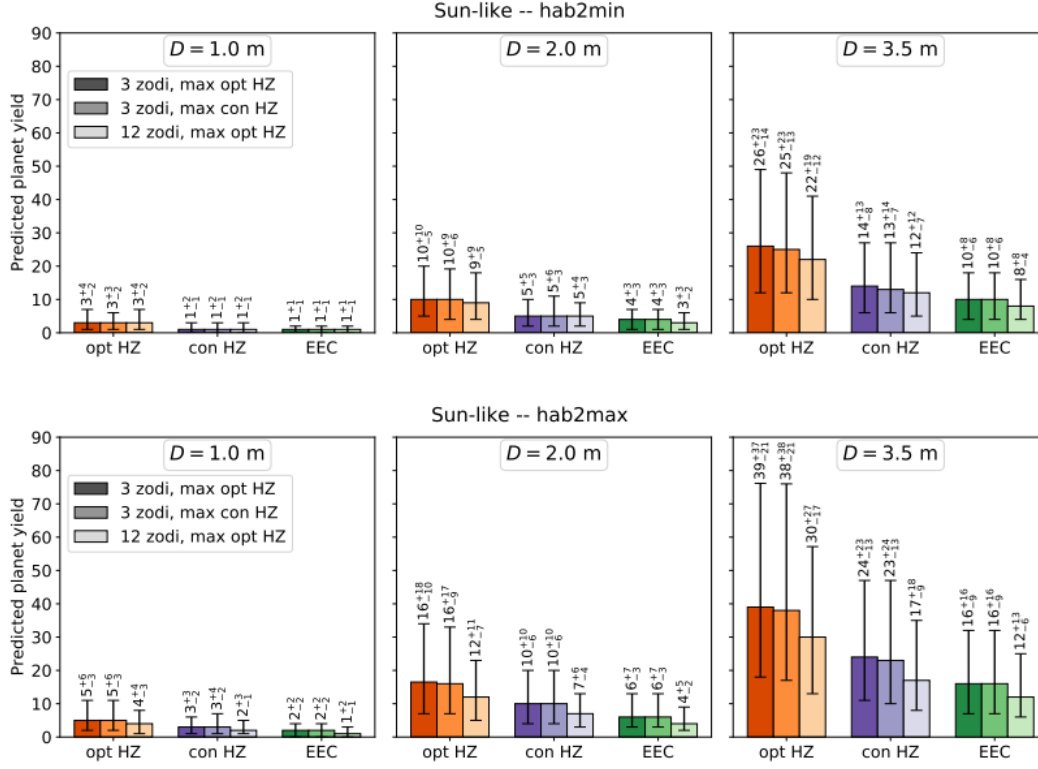Figure 14: Flowchart summarizing Kammerer et al. (2022).

Figure 15: Predicted planet yield for Sun-like stars. Each panel shows how many planets are expected to be detected under three different habitable zone (HZ) definitions (different colors) and three different observing scenarios (different shading): (1) median exozodiacal dust of 3 zodi, baseline optimized for the center of the optimistic HZ, (2) median dust of 3 zodi, baseline optimized for the center of the conservative HZ, and (3) median dust of 12 zodi, baseline optimized for the center of the optimistic HZ. The top row uses the hab2min planet population and the bottom row uses hab2max. Columns correspond to telescope mirrors of 1 m, 2 m, and 3.5 m (left to right).

Targets

Nearby Sun-like (4800–6300 K) and FGK (3940–7220 K) stars within 20 pc.

Exoplanet Yield

Aperture / Collectors	Rocky planets (0.5–1.5 $R_\oplus$)	Exo-Earth candidates (EECs)	HZ definitio
4 × 1 m	5–10	1–3	Optimistic H
4 × 2 m	10–16	4–6	Optimistic H
4 × 3.5 m	16–25	5–12	Optimistic H

Table 7: Rocky HZ planet yields for Kammerer et al. (2022) including FGK / Sun-like targets within 20 pc.

Conclusions & implications

Detecting a statistically useful sample of rocky HZ planets around Sun-like stars requires larger mirrors or higher throughput; LIFE concept (in baseline configurations) can deliver significant yields, and the dependence on throughput and aperture is emphasized for mission design tradeoffs.

Limitations & uncertainties

Extrapolations of Kepler occurrence rates to different stellar populations and to longer periods carry uncertainties; instrument performance and realistic noise budgets will impact final yields.

8   Comparative Overview of LIFE Mission Studies

The seven studies summarized in this document investigate the scientific potential of the LIFE mission using different assumptions, parameter choices, and analysis methods. **Kammerer & Quanz (2018)** present the **first exoplanet yield estimates based on Kepler occurrence rates**, using simplified blackbody planet models and idealized instrument assumptions; the most important result is the **strong sensitivity of predicted yields to habitable-zone definitions**, exozodiacal dust levels, and interferometer aperture size. **Kammerer et al. (2022)** focus specifically on rocky planets in the habitable zones of Sun-like stars and introduce more realistic noise terms, detection thresholds, and target selection criteria, demonstrating that detecting Earth-sized planets remains feasible for a significant number of nearby targets. **Quanz et al. (2021)** improve yield predictions through end-to-end mission simulations that include updated occurrence rates, optimized interferometric baselines, and detailed mission architectures, showing that LIFE could detect dozens of terrestrial planets under realistic observing conditions.

   Glauser et al. (2024) shift the emphasis from yield estimation to mission architecture and instrumental performance, identifying null depth, baseline stability, and formation-flying precision as key limiting parameters for LIFE. **Angerhausen et al. (2023)** investigate atmospheric characterization by modeling the detectability of phosphine (PH_3) for different planet types, atmospheric compositions, and integration times, highlighting the strong dependence of biosignature sensitivity on both planetary atmospheres and stellar environments. **Alei et al. (2024)** demonstrate the scientific value of combining LIFE thermal-emission spectra with reflected-light observations, showing that joint retrievals significantly improve constraints on planetary radius, temperature, and atmospheric composition compared to single-technique observations. Finally, **Angerhausen et al. (2025)** use Bayesian inference to assess the information content of null-result surveys, demonstrating that even non-detections can place strong statistical constraints on planet occurrence rates, with results depending critically on the assumed prior distributions and number of observed targets.

   Collectively, these papers show that LIFE's scientific return is determined by a combination of astrophysical assumptions, instrument design choices, observing strategies, and statistical interpretation methods.

References

[1] J. Kammerer & S. P. Quanz, "Simulating the exoplanet yield of a space-based mid-infrared interferometer based on Kepler statistics", A&A 609, A4 (2018). `https://arxiv.org/abs/1707.06820`

[2] S. P. Quanz et al., "LIFE I: Improved exoplanet detection yield estimates for a large mid-infrared space-interferometer mission", arXiv:2101.07500 (2021). `https://arxiv.org/abs/2101.07500`

[3] A. M. Glauser et al., "The Large Interferometer for Exoplanets (LIFE): a space mission for mid-infrared nulling interferometry", SPIE Proc. 13095 (2024). `https://orbit.dtu.dk/files/380743586/130951D.pdf`

[4] D. Angerhausen et al., "LIFE VIII: Where is the phosphine?", arXiv:2211.04975 (2022/2023). `https://arxiv.org/abs/2211.04975`

[5] E. Alei et al., "LIFE XIII: The value of combining thermal emission and reflected light for the characterization of Earth twins", A&A 664, A1 (2024). `https://arxiv.org/abs/2406.13037`

[6] D. Angerhausen et al., "What if we find nothing? Bayesian analysis of the statistical information of null results in future exoplanet habitability and biosignature surveys", AJ 169, 5 (2025). `https://arxiv.org/abs/2504.06779`

[7] J. Kammerer et al., "LIFE VI: Detecting rocky exoplanets in the habitable zones of Sun-like stars", A&A 668, A52 (2022). `https://arxiv.org/abs/2210.01782`